JAST, Vol. 12, No. 2, pp. 1- 11

JAST
Journal of Aerospace Science and Technology

Fatigue Life Assessment of Composite Airplane Wing Subjected to Variable Mechanical and Thermal Loads

A. Ebadi[1] and E. Selahi[2]*

1, 2. Department of Mechanical Engineering, Marvdasht Branch, Islamic Azad University

*Postal Code: 73711-13119, Marvdasht, IRAN

selahi@miau.ac.ir

The purpose of this paper is to estimate the fatigue life of an airplane wing with laminated composite skin, subjected to variable mechanical and thermal loads. To achieve this aim,at first, the three-dimensional model of airplane wing was drawn in CATIA software. Then, by transferring the model to the ABAQUS software, the finite element model of the wing wascreated. Here, the spars and ribs weremade ofaluminum T7075 and skin waslaminated composite with uni-directional and woven roving carbon epoxy layers. The convergence behavior of the structure wasexamined for selecting an appreciate element numbers. Finally, transient dynamic analysis followed by fatigue analysis of the wing structure was carried out. By performing fatigue simulation, the number of loading cycles resulted in failure of the structural components and wing skin panel was predicted. By comparing the simulation results with experimental research carried out by other researchers, the validity of the presented simulation method was demonstrated. The results of this research indicated that the replacement of traditional metallic wing skin with laminated composite skin causes a significant increase in fatigue life of the wing,besides a considerable weight reduction.

Keywords: Airplane wing, Composite skin, Fatigue life, Mechanical and thermal loads, Finite element method

Introduction

In the classic and modern design principles, designingthe wings is one of the first steps in manufacturingan airplane. Due to the fundamental role of wings in the production of lift force, the design and analysis of the wings is one of the most important issues in whichan airplane designer is involved. The wing structure under different maneuvers is exposed to various loads. Therefore, variable stresses are created alternatively in different components of this structure. These periodic loadsgradually reduce the strength of the wing structure, which results in the failure of these components instresses less than their static strength.

Also, planes are alternatively exposed to temperature reduction during flight and temperatureincrement on the ground. This leads to thermal fatigue as well as creation of thermal stresses. Therefore, considering the effect of alternating temperature changes on the airplane wings life andperforming thermal fatigue analysis is very important to estimate the loss of aircraft life. Aluminum is typically used for construction of airplanes structures. The reason for the use of aluminum in the aircraft structure is itsrelatively low density compared to steel and an appropriate strength to density ratio. Recently, in order to further reduce the weight of the aircraft and also increase the strength-to-weight ratio, the tendency to use carbon fiber composite materials in the fuselage, tail and wing structures has increased significantly. In recent years, considerable efforts

1. M.Sc. Graduate
2. Assistant Professor (Corresponding Author)

have been devoted to investigate the behavior of the wings:

In 1987, Thuresson and Abelin[1] performed the fatigue test on a composite wing of MFI-18 high-lift aircraft. Librescu and Nosier [2] investigated the response of fibrous composite plates subjected to sonic boom and explosive blast loading. The instability of a fully composite wing was investigated by Shokrieh and Taheri Behrooz in 2001 [3]. Hadadpoor and his colleagues examined aeroelasticinstability of the composite wings of aircraft in an incompressible flow [4].

Gomez [5] performed a numerical analysis of composite wings made of carbon fibers.Ozozturk [6]in his master's thesis analyzed the composite tactical unmanned air vehiclestructure made of carbon fiber and epoxy resin. Chitte andJadhav [7] employed Nastran finite element software to simulatestatic and dynamicalbehaviorof typical wing structure. They used shell elements for skin and beam elements for spars and ribs. They also examined the effects of thickness of the longitudinal spars on theirdisplacement and stress variations. Zhang et al. [8] applied a numerical simulation to design and optimize the composite wing structure of the minitype unmanned aerial vehicle. Kennedy and Martins [9] compared and optimized the design of the wing by replacing metal wings with composite wings. Kuntjoroet al.[10] used super-element,in finite element simulation to analyzethe stresses ina wing structure. Harakare andHeblikar[11], employed finite element approach and evaluated the static strength and critical buckling load of a wing box.They showed that the buckling does not occur in the wing box in normal loading conditions. Splichal et al.[12] investigated the dynamical behavior of composite wing skin experimentally. Detection, inspection, and failure analysis of the composite wing skin of a tactical airplane was carried out by Müller et al. [13].Chowdhury et al. [14] studied bolted, bonded and hybrid step lap joints of thick carbon fiber/epoxy panels used in the aircraft structures, experimentally and numerically.

In the design and construction of aircraft wings, after mechanical fatigue load and its stresses, the thermal fatigue and its thermal stresses caused by the alternating temperaturealso have great importance.

To the best of the author's knowledge, to-date there has beenno published study on the simultaneousthermal and mechanical fatigue analysis of composite airplane wing.Therefore, inthis research, by employing Abaqus finite element software, thefatigue lifeof composite airplane wing subjected to variable mechanical and thermal loads is estimated.

Modeling Method

The assumptions used in this simulation are as follows:

- In the fatigue analysis,the period and amplitude of mechanical and thermal loads remain constant.
- The perfect bond (Tie constraint) is used to attach skin to the wing structure.
- The beginning of the spar beams isconnected to the stiff and thick bulkhead of the fuselage. Therefore,fixed boundary condition is selected for this connection point.
- The finite element coupled Temperature-Displacement is carried out in a transient state.
- Thegeometrymodeling and analysis of the aircraft engine and fuel tanks are ignoredand only their weightsare applied inthe appreciate places.
- Materials behavior (whether composite or aluminum) are considered as linear elastic.
- Aluminum has isotropic material behavior and laminated composites haveorthotropic behavior.

Here, in additiontoapplying lift, drag and structural weight (as shown in Fig. 1), the engine and fuel weights are applied to the wing structuresto increase the accuracy of the wing airplane modeling.

In Fig. 2, an image of the wing structuredrawn in Catia software is shown and Table 1, illustrates the geometric characteristics of the selected wing.

The three-dimensional model of the wing plane is drawn inCatia software as follows:

In the first step, the internal structure of the wing consisting of spars and ribs isdrawn as shown in Fig. 3.

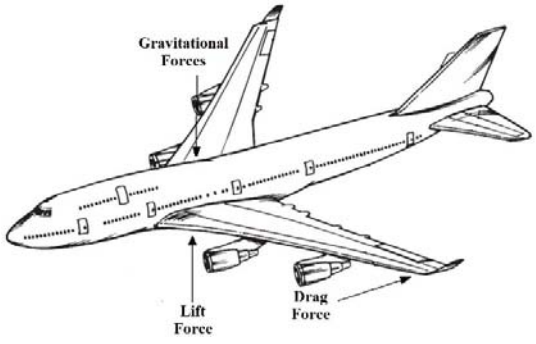

Figure 1. Gravitational, lift and dragforces [15]

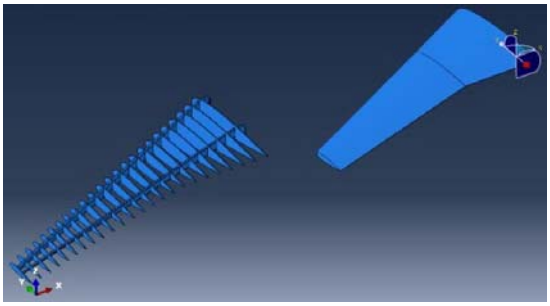

Figure 2. The drawing of the skin and wing structure

Table 1. Geometric characteristics of the wing [11]

Parameter	Value
Wing length	14 m
Length of the chord atthe wing root	6 m
Chord length atbreak section	3.75 m
Chord length atthe tip of the wing	1.8 m
Cone ratio (C_{tip}/C_{root})	0.3
Number of longitudinal spars	2
Number of transverse ribs	27
Distance from break section to root	4.5 m

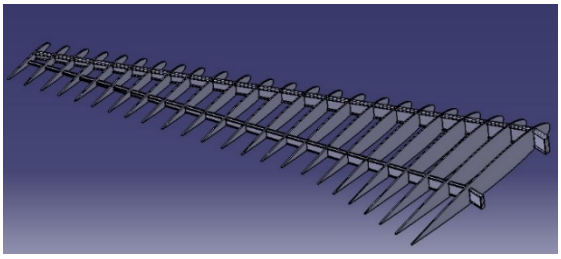

Figure 3. Internal wing structure

Then, the wing skin is plotted on the internal structure as shown in Fig. 2. Finally, the entire 3-D model is transferred to Abaqus finite element software.

In this modeling, all of the internal wing structures such as spars and ribs are made of aluminum T7075 with theroom temperature mechanical and thermal properties as shown in Table 2.

Table 2. Mechanical and thermal properties of aluminum T7075 at room temperature [16]

Properties	Value	Unit
Density	2710	Kg m^{-3}
Yield stress	516	MPa
Poisson coefficient	0.33	-
Tensile strength	587	MPa
Ultimate strain	9.1	%
Modulus of elasticity	72	GPa
Thermal expansion coefficient	23	µm/m-k
Thermal conductivity	130	W/m-k
Specific heat capacity	870	J/kg-k

Table 3. Mechanical and thermal properties of unidirectional carbon-epoxy composite at room temperature [16]

Properties	Value	Unit
Density	1490	Kgm^{-3}
Modulus of elasticity X	121	GPa
Modulus of elasticity in Y	8.6	GPa
Modulus of elasticity in Z	8.6	GPa
Poisson ratio XY	0.27	-
Poisson ratio YZ	0.4	-
Poisson ratio XZ	0.27	-
XY Shear Module	4.7	GPa
YZ Shear Modulus	3.1	GPa
XZ Shear Module	4.7	GPa
Tensile strength X direction	2230	MPa
Tensile strength Y direction	29	MPa
Tensile strength Z direction	29	MPa
Compressive strength X direction	-1082	MPa
Compressive strength Y direction	-110	MPa
Compressive strength Z direction	-110	MPa
Shear Strength XY	60	MPa
Shear Strength YZ	32	MPa
Shear Strength XZ	60	MPa
Thermal expansion coefficient X	4.7×10^{-7}	c^{-1}
Thermal expansion coefficient Y	3×10^{-5}	c^{-1}
Thermal expansion coefficient Z	3×10^{-5}	c^{-1}
Thermal conductivity	78.8	W/mk
Specific heat capacity	1130	J/kg-k

Table 4. Mechanical and thermal properties of woven roving carbon-epoxy composite at room temperature [16]

Properties	Value	Unit
Density	1420	Kgm^{-3}
Modulus of elasticity X	61.3	GPa
Modulus of elasticity in Y	61.3	GPa
Modulus of elasticity in Z	6.9	GPa
Poisson ratio XY	0.04	-
Poisson ratio YZ	0.3	-
Poisson ratio XZ	0.3	-

Properties	Value	Unit
XY Shear Module	19.5	GPa
YZ Shear Modulus	2.7	GPa
XZ Shear Module	2.7	GPa
Tensile strength X direction	805	MPa
Tensile strength Y direction	805	MPa
Tensile strength Z direction	50	MPa
Compressive strength X direction	-509	MPa
Compressive strength Y direction	-509	MPa
Compressive strength Z direction	-170	MPa
Shear Strength XY	125	MPa
Shear Strength YZ	65	MPa
Shear Strength XZ	65	MPa
Thermal expansion coefficient X	2.2×10^{-6}	c^{-1}
Thermal expansion coefficient Y	2.2×10^{-6}	c^{-1}
Thermal expansion coefficient Z	1×10^{-5}	c^{-1}
Thermal conductivity	78.8	W/mk
Specific heat capacity	1130	J/kg-k

In the design of the composite wing skins,carbon fibers laminated in two cases of: unidirectional fiber strand and woven roving fabrics with epoxy resin are used. Tables 3 and 4, listed the mechanical and thermal properties of unidirectional and woven roving of carbon-epoxy composite laminates, respectively.

The following stacking sequences areconsidered for design of the composite wing skin: $[0^{\text{Carbon Uni}}/\,0,90^{\text{Carbon Woven}}/\,0^{\text{Carbon Uni}}/0,90^{\text{Carbon Woven}}/\,0^{\text{Carbon Uni}}]$

The thickness of each layer is 0.4 mm.It is worth mentioning that woven fabrics with 45° layout used to withstand shear stresses and unidirectional fibers, were selected to withstand normal stresses along the longitudinal and transverse directions of the wings.To compare the performance of a composite wing skin with a common aluminum skin, the described fatigue analysis for the wing with 2 mm aluminum skin thickness is also carried out.

In this research, 3-node triangular shell element for laminated skin and 4-node tetrahedron solid elements are usedfor meshing the ribs and spars.

Here, the applied mechanical and thermal loads are functions of time; therefore, their responses such as temperature, displacement, strain, and stress are also time-dependent.The following loads are applied on the wing structure:

- Wing weight (including: wing structure and skin weight)
- Aircraft engine weight
- Fuel and its tanksweight
- Lift and drag forces
- Temperature variation loads

The first three forces are gravitational forces that are considered to be constant.The second last forces are alternating dynamic loads andeach loading cycle is introduced in three steps as follows:

The first stage is park of the aircraft on the runway with an empty fuel tank andat the temperature of 25° C.

The second stageis the horizontalflight at a steady speed of 870 km/h and temperature of -40 °C. In this case, the resultant of drag and thrust forces is equal to zero. Also,the weight of the tanks, motor weight and other gravitational forces are calculated and applied.

The last stage is the landing of the aircraft at a speed of 240 km/h and at temperature of 25 °C.In this case, the thrust force is negligible compared to the drag force. Also, all gravitational forces are considered in this stage.

Table 5 presented the capacity of all airplane fuel tanks.

Table 5. Capacity of fuel tanks in the aircraft [17]

Tank	Capacity (liter)
The inner tank of the wing / right	6924
The inner tank of the wing / left	6924
External reservoir of wing / right	880
External reservoir of wing / left	880
Central reservoir	8250

The weight of the fuel tanks in a perfectly filled state, as shown in Fig. 4, isapplied as distributed loads on spars and ribs. The weight of the aircraft engine is 2190 kg. According to Fig. 5, this weight force is applied as distributed loads onparts of the spars and ribs.

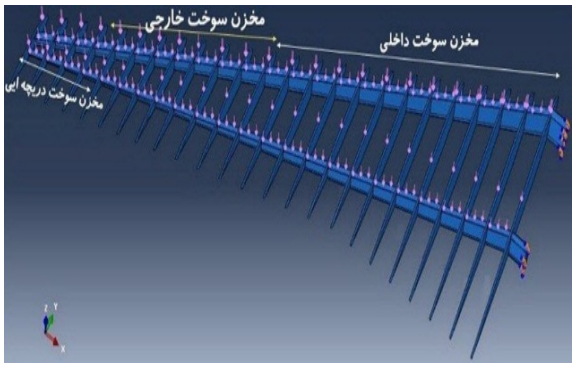

Figure 4. Location of applying the gravitational fuel tanks forces

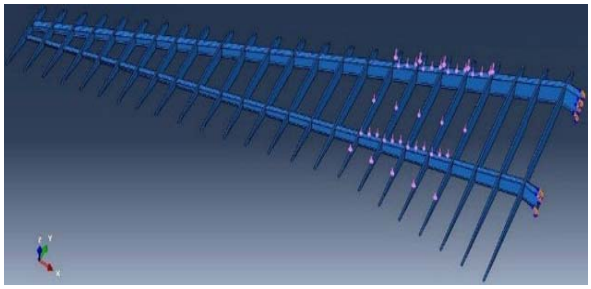

Figure 5. Location of applying the engine weight

Fig.s 6 and 7 illustrated the diagrams of strength-fatigue life and strength vs. temperature of aluminum T7075, respectively. Moreover,in Fig.s 8 and 9, the diagrams of strength percentage -fatigue life and strength percentagein terms of temperature for carbon-epoxy composite areshown, respectively. It should be noted that the diagrams presented in Fig.s 9 and 10 can be applied to each of the nine strength components of the orthotropiccarbon-epoxy composite.

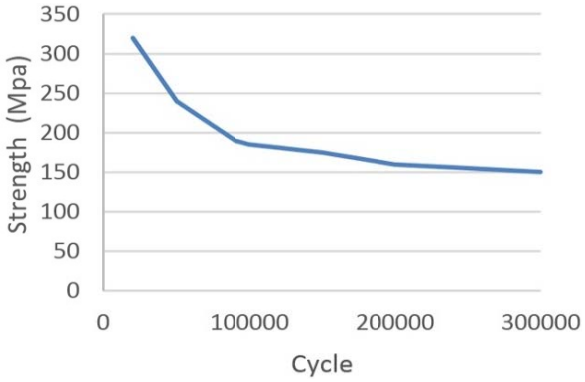

Figure 6. Strength-fatigue life diagram of aluminum T7075 [18]

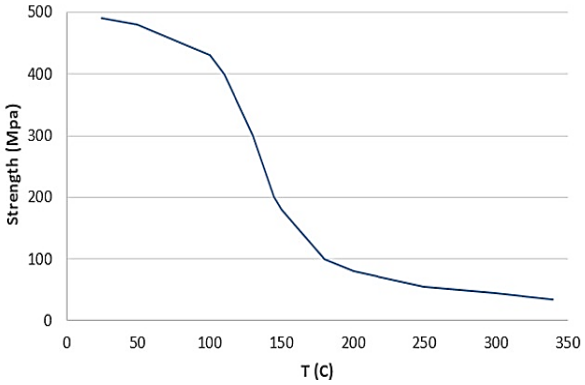

Figure 7. Strength-temperature diagram of aluminum T7075 [19]

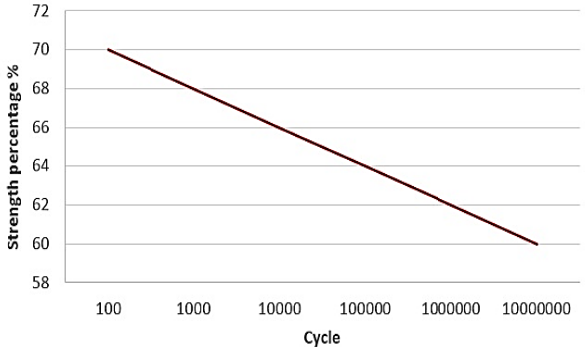

Figure 8. Strength percentage-fatigue life diagram of carbon-epoxy composite [20]

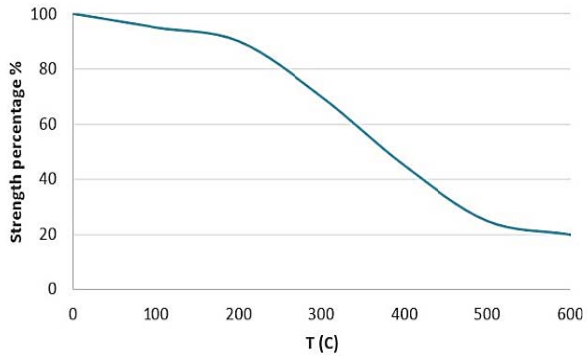

Figure 9. Variations of strength percentage in terms of temperature for carbon-epoxy composite [20]

The dynamicstress results areextended to estimate the stress variations in the higher cycles.By using strength-fatigue life and strength-temperature diagrams presented in Fig.s6 to 9and comparing them with dynamicstress results, thefatigue lifefor different components of the wings are calculated.

In order to predict the fatigue failure ofthe aluminum structures, the Von-misesequivalent stress is used.Hashin's criterion [21] in accordance with Equations (1) to (4)was used to predict the fatigue failure of the composite skin.

1. Tensile fiber failure for $\sigma_1 \geq 0$

$$\left(\frac{\sigma_1}{X_T}\right)^2 + \frac{\sigma_{12}^2 + \sigma_{13}^2}{S_{12}^2} = \begin{cases} \geq 1 & failure \\ < 1 & no\ failure \end{cases} \qquad (1)$$

2.Compressivefiber failure for $\sigma_{11} < 0$

$$\left(\frac{\sigma_1}{X_C}\right)^2 = \begin{cases} \geq 1 & failure \\ < 1 & no\ failure \end{cases} \qquad (2)$$

3. Tensile matrix failure for $\sigma_2 + \sigma_3 > 0$

$$\frac{(\sigma_2+\sigma_3)^2}{Y_T^2}+\frac{\sigma_{23}^2-\sigma_2\sigma_3}{S_{23}^2}+\frac{\sigma_{12}^2+\sigma_{13}^2}{S_{12}^2}=\begin{cases}\geq 1 & failure\\ <1 & no\ failure\end{cases} \quad (3)$$

4. Compressive matrix failure for $\sigma_2+\sigma_3<0$

$$\left[\left(\frac{Y_C}{2S_{23}}\right)^2-1\right]\left(\frac{\sigma_2+\sigma_3}{Y_C}\right)+\frac{(\sigma_2+\sigma_3)^2}{4S_{23}^2}+\frac{\sigma_{23}^2-\sigma_2\sigma_3}{S_{23}^2}+\frac{\sigma_{12}^2+\sigma_{13}^2}{S_{12}^2}=\begin{cases}\geq 1 & failure\\ <1 & no\ failure\end{cases} \quad (4)$$

where: σ_1,σ_2 and σ_3 are stress components in directions 1, 2 and 3 , respectively, σ_{12},σ_{13} and σ_{23} are shear stress components, X_T, X_C, Y_T and Y_C are tensile and compressive strength components in directions 1 and 2, respectively, and $S_{12}S_{13}$, and S_{23} are shear strength components.It is noticeable that all of the strength and stress components are dependent on the number of loading cycles and temperatures.

In Fig. 10, applying thermal load in the second and third stages of a cycle consisting ofhorizontallight at temperature of -40 °C, and a landing of the aircraft at temperature of 25 °Careshown.

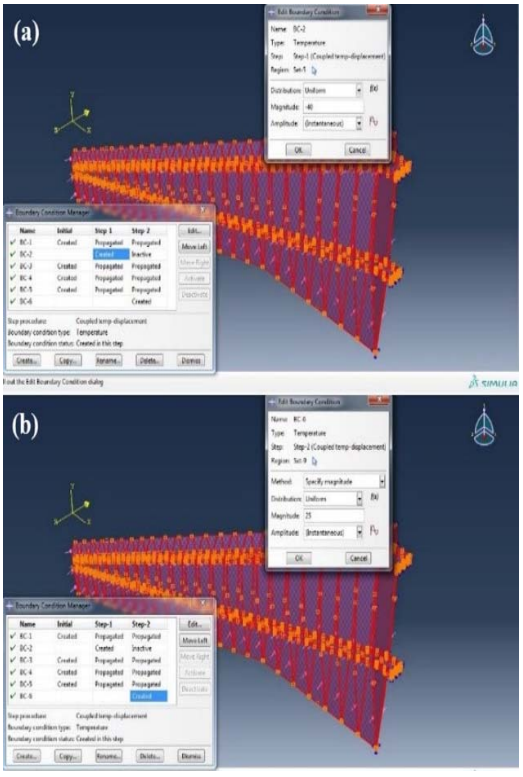

Figure 10. Applying thermal load in (a) horizontal flight and (b) landing stages

Results

Validation

Due to the lack of experimental resultsfor laminated composites exposed to mechanical and thermal fatigue loads, the validation and confirmationaccuracy of the presented simulation werecarried out by comparing the results of fatigue modeling performed by Abaqus software with the obtainedexperimental results subjected to thermal fatigue and mechanical loads presented in [22]. The material of the specimen is Inconel 617 covered by the plasma air method. Fig. 11, described the geometry of the specimen.

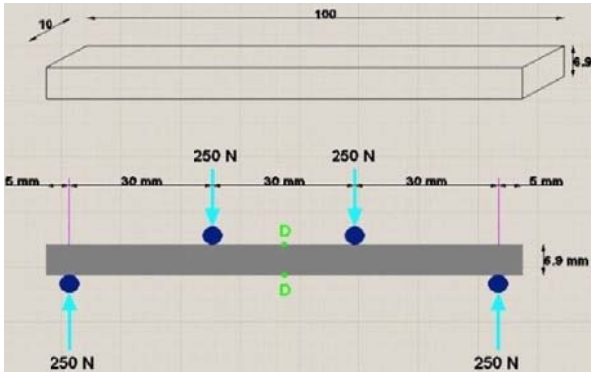

Figure 11. Geometric specifications of the specimen [22]

According to Fig. 11, the specimen is subjectedto bending load with the maximum bending moment of 7500N. mm. The specimen is also exposed to the alternating temperature variation between 0 to 1170 C°. In Fig. 12, the time variations diagram of the specimen temperature is plotted in one thermal cycle.

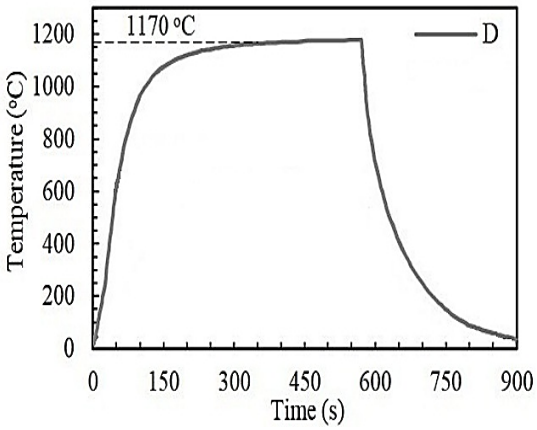

Figure 12. Temperature variations of the sample in terms of time in one thermal cycle [22].

Table 6listed the strength of the specimen in terms of temperature.

Table 6. Tensile strength of Inconel 617 in terms of temperature [22]

Temperature (C°)	Strength (Mpa)
0 – 150	755
150 – 595	769
595 – 650	789
650 - 1200	872

The temperature variations of mechanical and thermal properties for the underlying layer, bonding coat, the aluminum oxide layer and the upper coating layerof the specimen are listed in Tables 7 to 11.

Table 7. Specific heat capacity, conductivity and density ofbonding coat NiCoCrALY [22]

Temperature (C°)	Density (Kg/m^3)	Temperature (C°)	Thermal conductivity (W/mK)	Temperature (C°)	Specific heat capacity (J/kgK)
24.9	6189	28.1	4.3042	21.3	542.9
300.3	5664	299.5	5.9646	251.7	659.2
500.3	5844	500.4	6.9534	499.6	712.1
710.9	6423	700.5	9.7197	698.6	738.5
900.5	6479	899.9	10.6836	901.1	757.5
1100.9	6521	1100.0	13.1745	1000.8	746.9
1200.3	6590	1200.7	16.1223	1198.8	772.0

Table 8. Specific heat capacity, conductivity and density of upper coating (ZrO2-8wt% Y2O3 (YSZ)) [22]

Temperature (C°)	Density (Kg/m^3)	Thermal conductivity (W/mK)	Specific heat capacity (J/kgK)
25	4820	1.4998	455.60
126.85	4820	1.4998	516.14
326.85	4820	1.4998	568.08
526.85	4820	1.4998	595.67
726.85	4820	1.4998	616.77
926.85	4820	1.4998	635.44
1126.85	4820	1.4998	652.48
1156.85	4820	1.4998	655.73
1176.85	4820	1.4998	719.84

Table 9. Modulus of elasticity, poisson ratio and thermal expansion coefficient of coating layers [22]

Temperature (C°)	Upper cover density(ZrO2-8wt%Y2O3(YSZ))			Dioxide layer (α-AL2O3)			Link overlay (NiCoCrALY)		
	Thermal expansion coefficient (1/C)	Poisson's ratio	Young's modulus (Gpa)	Thermal expansion coefficient (1/C)	Poisson's ratio	Young's modulus (Gpa)	Thermal expansion coefficient (1/C)	Poisson's ratio	Young's modulus (Gpa)
20	$9.68*10^{-6}$	0.2	17.5	$5.08*10^{-6}$	0.27	380.37	$1.24*10^{-5}$	0.3189	151.86
220	$9.68*10^{-6}$	0.2	16.34	$5.90*10^{-6}$	0.27	369.06	$1.30*10^{-5}$	0.3271	150.75
420	$9.71*10^{-6}$	0.2	15.18	$6.73*10^{-6}$	0.27	361.23	$1.39*10^{-5}$	0.3343	145.25
620	$9.81*10^{-6}$	0.2	14.02	$7.55*10^{-6}$	0.27	351.88	$1.50*10^{-5}$	0.3409	132.34
820	$1.00*10^{-5}$	0.2	12.86	$8.38*10^{-6}$	0.27	336.03	$1.62*10^{-5}$	0.3466	108.92
1020	$1.04*10^{-5}$	0.2	11.7	$9.20*10^{-6}$	0.27	308.71	$1.77*10^{-5}$	0.3515	71.89

Table 10. Specific heat capacity, conductivity and density ofoxide layer (α-AL2O3) [22]

Temperature (C°)	Density (Kg/m^3)	Thermal conductivity (W/mK)	Specific heat capacity (J/kgK)
20	3984	33.00	755
500	3943	11.40	1165
1000	3891	7.22	1255
1200	3863	6.67	1285

Table 11. Mechanical and thermal properties of the Inconel 617 [22]

Temperature C	Density Kg/m^3	Thermal conductivity W/mK	Special heat capacity (J/kgK)	Expansion coefficient (1/C)	Poisson's ratio	Young's modulus (Gpa)
25	8360	13.5	420	--	0.30	211
100	8360	14.7	440	$1.16*10^{-5}$	0.30	206
300	8360	17.7	490	$1.31*10^{-5}$	0.30	194
500	8360	20.9	536	$1.39*10^{-5}$	0.30	181
700	8360	23.9	586	$1.48*10^{-5}$	0.30	166
900	8360	27.1	636	$1.58*10^{-5}$	0.30	149
1000	8360	28.7	662	$1.63*10^{-5}$	0.31	139
1100	8360	--	--	--	0.32	129

Finite element modeling in Abaqus software iscarried outforthe similar cyclic thermal loading and flexural load conditions with the experimental resultsare presented in [22]. In Fig. 13, the variations of safety factors in terms of cycle numbers calculated by thermal fatigue analysis in Abaqus softwareareshown.

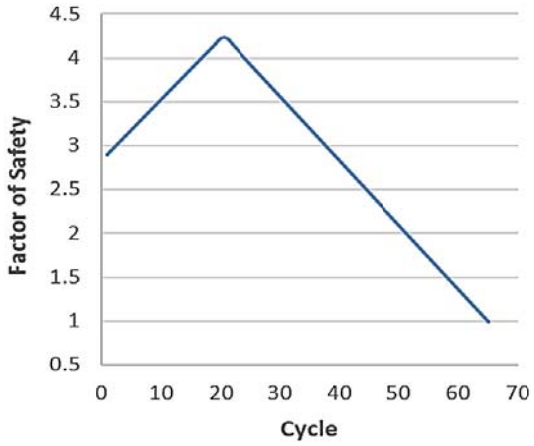

Figure 13. Factor of safety in terms ofthe thermal cycle numbers

According to the finite element modeling results, failure occurs in the 65th cycle. While the experimental test results showed a failure in the 64th thermal cycle number.Therefore, the difference between simulation results and experimental resultsisonly 1.5%, which indicates the high accuracy of the simulation method.

Convergence Study

In this section, theconvergence study is carried out to choose theoptimal element numbers in the fatigue analysis of the wing. Here, by changing the size of the elements and subsequently, increasing or decreasing the number of elements used in the modeling, the sensitivity of the structure on the maximum Von-mises stress was studied in terms of the elementnumbers.

Table 12, listed the maximum magnitude of Von-mises stress occurred in the internal structure in terms of element numbers.

Table 12. Maximum magnitude of Von-mises stress in terms of element numbers

Case	Number of elements	Maximum Von-mises stress (MPa)
1	567316۵	97.0
2	579523	98.4
3	598229	100.2
4	618936	102.1
5	637760	105.3
6	656770	105.3

It is observed that, the maximum Von-mises stressin the 5th case is equal to the 6th case. Therefore, the 5thcase with 637,760 total elements numbers was selected.

Fatigue Analysis Results

Due to the long period of a loading cycle, the structure will have enough time to return to the proportional position with the load magnitude. In other words, by increasing the number of loading cycles, the magnitudes of deformation and stress componentsdonot change in the similar positions and stages and they are repeated identically.

The modeling of wing structures ispresented in two cases as follows: (1) fully aluminum wing and (2) composite wing skin with internal aluminum structures.

At first, the results of fully aluminum wing will be presented. According to Fig. 14, the fatigue life of the wing structure was calculated by comparing the strength-fatigue life diagram of aluminum T7075 (Fig. 6) with the maximum Von-mises stress at the critical point of the aluminum structure.

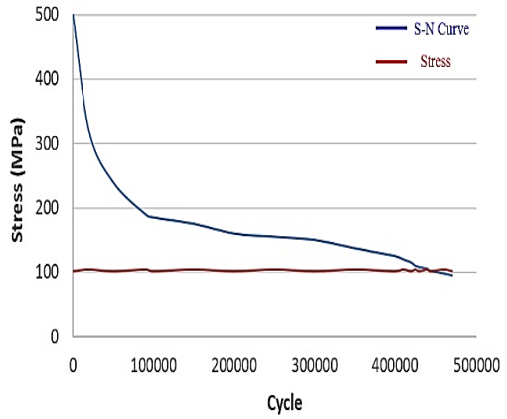

Figure 14. Determination of fatigue life forthe aluminum structure at the critical point of the spars in the fully aluminum wing

It was observed that the aluminum structure began to fail after 443267 loading cycles. Similarly, in Fig. 15, the fatigue life of the aluminum wing skin was calculated by comparing the strength-fatigue life diagram of aluminum T7075with the maximum Von-mises stress developed at the critical point of the aluminum skin. Diagrams of Fig. 15depicted that the failure of the aluminum skin is initiated after 335764 loading cycles.

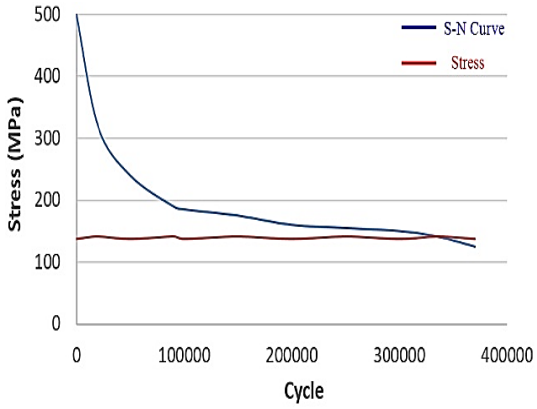

Figure 15. Determination of fatigue life for aluminum skin in the fully metallic wing

Here, the results of fatigue analysis for composite wing with an aluminum structure and 5-layer carbon-epoxy skin arepresented. Fig. 16 depicted the Von-mises stress contour in the aluminum ribs and spars andin Fig. 17, the contour of Hashin'scriteria in the case of tensile fiber failure, for the laminated composite wing skin is shown. All of these contours are presented for the second loading stage.

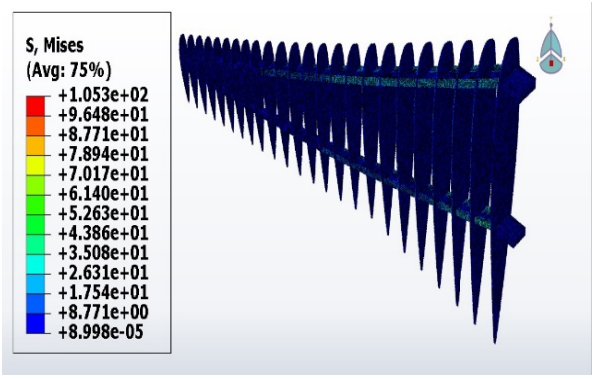

Figure 16. Von-mises stress contour in the aluminum ribs and spars

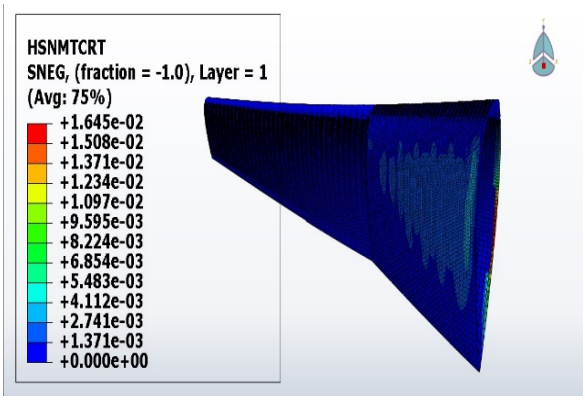

Figure 17. Hashin's criteria contour in the case of tensile fiber failure, for the laminated composite wing skin

In Fig. 18, the strength-fatigue life diagram of aluminum is compared to the Von-mises stress diagram at the critical point of the aluminum structure. Table 13listed the Hashin's criteria in the four-state failure defined in equations 1 to 4, at the critical point of the compositeskin in terms of the cycle number.

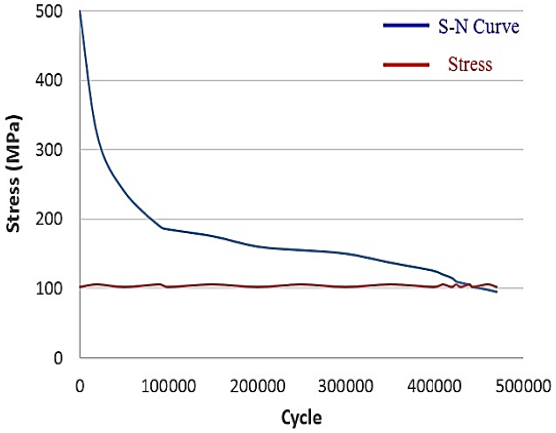

Figure 18. Fatigue life determinationfor critical point aluminum spars in the composite wing

According to the results of Table 13, after 908611 loading cycles,the critical point of the laminated composite skin began to rupturedue to tensile fiber failure mode.

Also, by comparing the diagrams of Fig.s 14 and 18, it is observed that replacing composite skininstead of aluminum skin, not only leads to increasein skin life, but also leadsto the enhancedlife of the aluminum ribs and spars up to 443267 cycles.

It is noteworthy that the critical condition happened in the same loading stage for both aluminum structures and composite skin.

In other words, by replacing the aluminum-skin with a carbon-epoxy laminated composite skin, in addition to a weight reduction of 48%, a 32% increase in fatigue life of the internal structure and a 270% increase in fatigue life of the wing skinoccurred.

Conclusion

In this study, a three-dimensional modeling of airplane wing including:spars, ribs andwing skin, was drawn with Catia software and transferred to Abaqus software.

Table 13. Hashin'sindex at the critical point of the composite skin

Cycle	Tensile fiber failure	Compressive fiber failure	Tensile Matrix failure	Compressive Matrix failure
1	$1.65*10^{-2}$	$5.09*10^{-4}$	$4.19*10^{-4}$	$2.09*10^{-4}$
50000	$3.89*10^{-2}$	$7.48*10^{-3}$	$6.94*10^{-4}$	$3.64*10^{-3}$
100000	$7.36*10^{-2}$	$3.56*10^{-2}$	$5.68*10^{-3}$	$1.36*10^{-2}$
130000	0.14	$7.53*10^{-2}$	$7.52*10^{-2}$	$7.52*10^{-2}$
180000	0.20	0.11	0.10	0.11
200000	0.22	0.12	0.11	0.12
440000	0.48	0.27	0.24	0.26
600000	0.61	0.32	0.30	0.31
700000	0.77	0.42	0.39	0.42
908611	1.00	0.55	0.51	0.55

To create the finite element modeling of the wing, three-dimensional solid elements were employed for the internal structures and shell elements were usedfor the wing skin.

In order to study the performance of composite wings compared to conventional aluminum wings, two design cases for the airplane wingwere analyzed.

The first design is the metallic wings made of aluminum T7075.In the second design, the ribs and spars are aluminum and the wing skin is made of laminated composite with 5 layers of carbon-epoxy.

Each loading cycle of the wing structure consists of the three following stages: 1. To park on the runway with an empty fuel tank, 2. To flyhorizontally at a constant speed and 3. To land the aircraft.In each cycle, alternating mechanical and thermal loads related to that condition were applied to the wing structure.

By studying the effect of element size on fatigue behavior of the wing structures, the suitable number of elements for modeling was selected.Also, the results of fatigue analysis calculated by Abaqus software are compared successfully with the experimental results of a specimensexposed to the mechanical load and thermal fatigue provided by other researchers.

By performing fatigue analysis of the wing under periodic mechanical and thermal loads, fatigue life of the internal structures and wing skin were estimated in both cases of aluminum and compositewings.

It was observed that the ribs and spars are the first segments of wing that suffer from fatigue failure. Also, replac ingaluminum skin with a carbon-epoxy composite skin, leads to a 48% weight reductionas well as a 32% increase in fatigue life of the internal structure and alsoa 270% increase in fatigue life of the wing skin.

References

[1] Thuresson, S., Abelin, R.,"Fatigue testing of an all-compositewing for the MFI-18 high-lift aircraft," *Composites*, Vol. 18, No. 4, 1987, pp. 334-338

[2] Librescu, L. and Nosier,A., "Response of laminated composite flat panels to sonic boom and explosive blast loading," *Journal of Aircraft*, Vol. 28, No.2, 1990, pp. 345-352.

[3]Shokrieh, M. M. and Taheri Behrooz, F., "Wing instability of a full compositeaircraft," *Composite Structures,* Vol. 54, No. 2–3, 2001, pp 335-340.

[4]Haddadpour, H., Kouchakzadeh, M. A. and Shadmehri, F., "Aeroelastic instability of aircraft compositewings in an incompressible flow," *Composite Structures*,Vol. 83, No. 1, 2008, pp. 93-99.

[5] Gomez, S. M., "Numerical analysis of carbon fibre reinforced aircraft wing*," International Journal of Earth Sciences and Engineering*, vol. 4, No. 6, 2011, pp. 648-651.

[6] Ozozturk, S., "Structural and analysis of a composite tactical unmanned air vehicle," Mastersthesis, Middle Eeast Technical Univesrsity, 2011.

[7] Chitte, P. and Jadhav, K., "Static and dynamic analysis of typical wing structure of aircraft using Nastran," *International Journal of application or*

Innovation in engineering and management, Vol. 2, 2013, pp.321-326.

[8]Zhang, Y., Xiong, F. and Yang, S., "Numerical simulation for composite wing structure design optimization of a minitype unmanned aerial vehicle," *The Open Mechanical Engineering Journal*, Vol. 5, 2011, pp.11-18.

[9]Kennedy, G. J. and Martins, J.R.R.A., "A comparison of metallic and composite aircraft wings using aero structural design optimization," *American Institute of Aeronautics and Astronautics*, 2012.

[10] Kuntjoro, W., Abduljalid. A. and Mahmud. J., "Wing structure static analysis using superelement," *Journal of procedia engineering*, Vol. 41, 2012, pp. 1600-1606.

[11] Harakare, P. and Heblikar, K.V., "Evaluation of static and buckling load carrying capability of the wing box through FEM approach," *International Journal of current engineering and technology*, 2013, pp. 6-9.

[12]Splichal, J., Pistek, A. andHlinka, J., "Dynamic tests of composite panels of an aircraftwing," *Progress in Aerospace Sciences,* Vol. 78, 2015, pp. 50-61.

[13]Mueller, E. M., Starnes, S., Strickland, N., Kenny, P. and Williams, Ch.,"The detection, inspection, and failure analysis of a compositewing skin defect on a tactical aircraft," *Composite Structures*,Vol. 145, 2016, pp.186-193.

[14] Chowdhury, N.M., Chiu, W. K., Wang, J. and Chang, P., "Experimental and finite element studies of bolted, bonded and hybrid step lap joints of thick carbon fibre/epoxy panels used in aircraft structures," *Composites Part B: Engineering,*Vol. 100, 2016, pp. 68-77.

[15] https://www.mansfieldct.org/Schools /MMS/staff/ hand/flight4forcesoverviewhtm.

[16] ANSYS Workbench V. 16. Engineering Data Sources.

[17] Rashidi, E. and Fazelzadeh, S.A., "Investigating the effect of aero-elastic loading model and roll-back angle on aircraft wing speed and frequency," *16th International (Annual) Conference of Mechanical Engineering, Kerman*, Iran, 2008 (in Persian).

[18] Oskouei, R. and Ibrahim, R. N.,"The effect of a heat treatment on improving the fatigue properties of aluminium alloy 7075-T6 coated with TiN by PVD," *Procedia Engineering*, Vol. 10, 2011, pp. 1940-1946.

[19]https://www.m4carbine.net/showthread.php?174986 -Should-the-gas-block-steel-match-the-barrel-steel.

[20] Greene E., *Marine Composites*, Eric Greene Associates, Second Edition, 1999.

[21] Hashin, Z., "Failure criteria for unidirectional fibre composites," *ASME Journal of Applied Mechanics*, Vol. 47, No. 2, 1980, pp. 329-334.

[22] Karaoglanli, A.C. and Ogawa, K., "Thermal Shock and Cycling Behavior of Thermal Barrier Coatings (TBCs) Used in Gas Turbines, *in Progress in Gas Turbine Performance*,"NITECH, 2013, pp. 237-261.